Supplemental Figures

Supplemental Figure 1

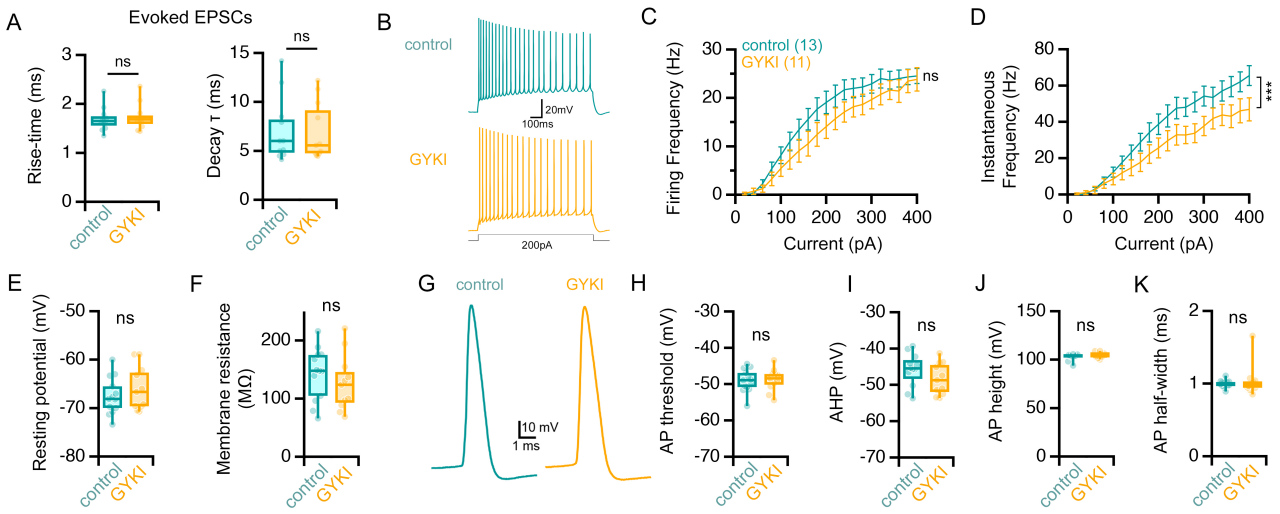

Supplemental Figure 1, related to Figure 1. GYKI does not increase the intrinsic excitability of CA1 pyramidal neurons.

(**A**) Rise-time and decay time constants for EPSCs evoked in the *stratum oriens* after 30 minute pre-incubation ± GYKI (5μM). control n = 10 cells from 5 mice; GYKI n = 11 cells from 5 mice. (**B**) Representative voltage traces of CA1 pyramidal neurons firing in response to a 200pA square pulse of depolarizing current. (**C-D**) Average firing frequency (*C*) and average instantaneous firing frequency of the first 4 actions potentials (*D*) in response to square pulse current injection from slices that have been pre-incubated ± GYKI (5μM). Data is mean (± SEM). (**E-F**) GYKI pre- incubation does not alter resting membrane potential (*E*) or membrane resistance (*F*). (**G**) Example voltage traces of action potential waveforms. (**H-K**) GYKI pre-incubation does not change the action potential threshold (*H*), after-hyperpolarization (AHP) voltage (*I*), height (*J*) or half-width (*K*). control n = 13 cells from 7 mice; GYKI n =11 cells from 7 mice (*C-K*).

ns p>.05; *** p<.005 Student's t-test, two-tailed (*A, E-F, H-K*) and two-way repeated measures ANOVA (*C,D*).

Supplemental Figure 2

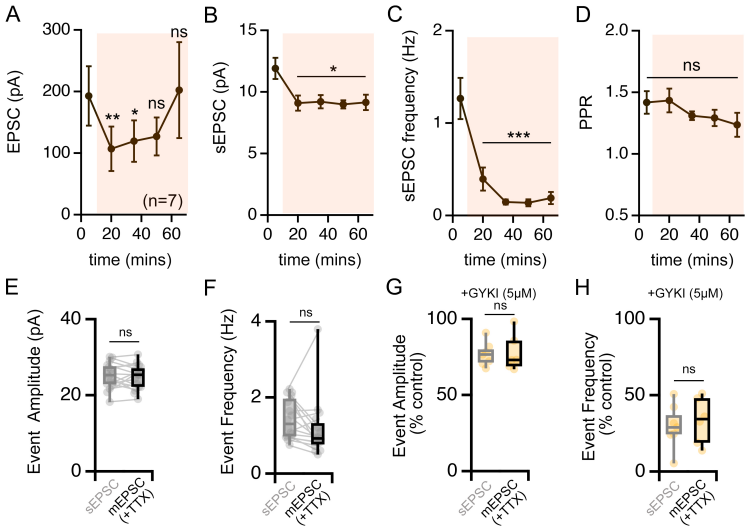

Supplemental Figure 2, related to Figure 1. The homeostatic recovery of evoked neurotransmission occurs in the absence of changes to spontaneous neurotransmission

(**A-D**) Raw values of data shown in Figure 1M-O. Data are mean (± SEM). n = 7 cells from 5 mice**.** (**E-F**) Amplitude (*E*) and frequency (*F*) of spontaneous (sEPSC) and miniature (mEPSC) release events. Spontaneous events were recorded for 10 minutes before tetrodotoxin (TTX; 0.5μM) was bath applied prior to the measurement of mEPSCs for an additional 10 minutes. n = 16 cells from 4 mice. (**G-H**) Relative amplitude (*G*) and frequency (*H*) of sEPSCs and mEPSCs recorded in the presence of GYKI (5μM). sEPSCs n = 8 cells from 4 mice; mEPSCs n = 6 cells from 2 mice.

ns p>.05; * p<.05; ** p<.01; ***p<.001, one-way repeated measures ANOVA and Dunnett's or Holm-Šídák multiple comparisons test (*A-D*), paired t-test, two-tailed (*E-F*), Student's t-test, two tailed (*G-H*).

Supplemental Figure 3

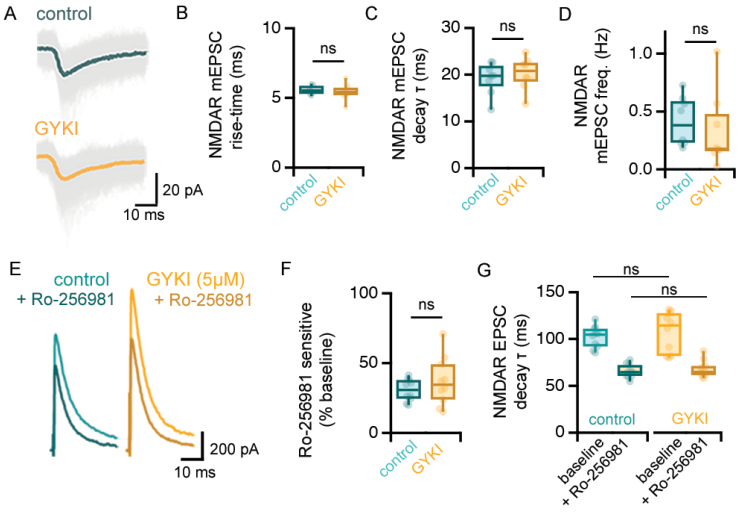

Supplemental Figure 3, related to Figure 2. Properties of NMDAR-mediated neurotransmission

(**A**) Representative traces of individual (grey) and mean (colour) NMDAR-mediated mEPSCs after a 30 minute incubation ± GYKI (5μM). Events were recorded in 0mM $[Mg^{2+}]_e$ at a holding potential of -70mV directly following bath application of NBQX (10μM). (**B-D**) Rise-time (*B*), decay (*C*), and frequency (*D*) of NMDAR-mediated mEPSC events. control n = 8 cells from 3 mice; GYKI n = 8 cells from 3 mice. (**E**) Representative traces of NMDAR-mediated evoked EPSCs before and after treatment with the GluN2B-specific antagonist, Ro-256981 (10μM). Evoked NMDAR-mediated EPSCs were recorded in 2.5mM $[Ca^{2+}]_e$ and 0.5mM $[Mg^{2+}]_e$ at a holding potential of +40mV in the presence of NBQX (10μM). (F) Percentage of Ro-256981-sensitive component of NMDAR-mediated EPSCs, normalized to baseline prior to Ro-256981 application. (**G**) The decay constant of NMDAR-mediated EPSCs before and after Ro-256981 treatment.

ns p>.05, Student's t-test, two tailed.

Supplemental Figure 4

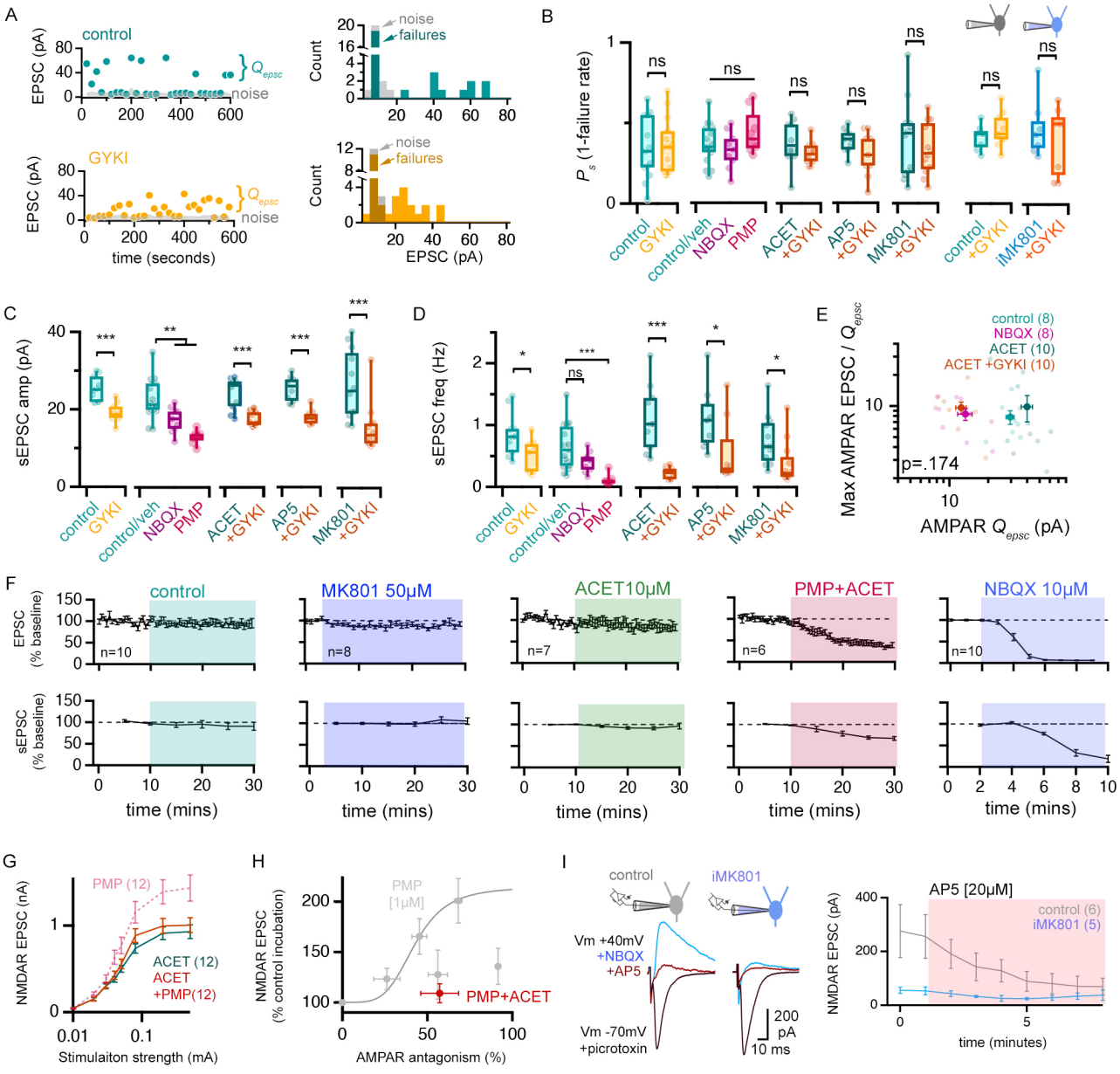

Supplemental Figure 4, related to Figure 2, 3. Calcium input/out paradigm and the glutamatergic neurotransmission at CA1 *stratum oriens* synapses

(**A**) EPSC amplitudes recorded over time (left) and resulting amplitude histograms (right) in low (0.5mM) external calcium ($[Ca^{2+}]_e$) enable estimation of Q_{epsc}. Stochastic release events are intermingled with failures of neurotransmission. The threshold for a successful release event was defined as 3X the standard deviation of the noise, measured 5 ms before the stimulus artifact. The average amplitude of successful release events is defined as Q_{epsc}. (**B**) The probability of observing a successful release event (P_s), as shown in *Figure 3*. Sample sizes are shown in Figure 3. In each cell, 30 sweeps of stimuli were delivered at 0.05Hz and used to determine P_s. (**C-D**) The amplitude (*C*) and frequency (*D*) of spontaneous EPSCs (sEPSCs) for data shown in *Figure 3*. (**E**) Single

experiments (light markers) and the resulting means (dark markers) for each pre-incubation condition indicated. Q_{epsc} were determined for each cell during a 10min in (0.5mM) $[Ca^{2+}]_e$. The max AMPAR EPSC is the average of the plateau in the calcium input-output plots shown in *Figure 3*. The p-value was determined for a Pearson correlation. The number of cells is shown in brackets and are obtained from at least 3 different mice. (**F**) Evoked EPSC and sEPSC amplitudes as a function of time and following addition of GluR antagonists to the bath (coloured boxes). Number of cells are shown from at least 3 different mice. (**G**) Stimulus input-output curves (mean ± SEM) representing NMDAR-mediated EPSCs in response to increasing stimulation strength. Data for PMP (1μM) is reproduced from *Figure 2D*. Number of cells is shown in brackets and obtained from at least 3 different mice. (**H**) Normalized NMDAR-mediated EPSCs following pre-incubation with GluR antagonists (as indicated) as a function Q_{epsc}. Graph is reproduced from *Figure 2F*, and includes data shown in this figure – panels *G* and F (i.e. PMP [1μM] +ACET [10μM]). The curve is reproduced from the Hill function shown in *Figure 2C*. (**I**) At left, representative traces of AMPAR-mediated EPSCs (Vm -70mV, isolated with picrotoxin [100μM]), NMDAR-mediated EPSCs (Vm +40mV, +NBQX [10μM]), and residual current after the addition of AP5 (20μM), measured with normal pipette solution and solution containing MK801 (iMK801; 1μM). At right, the time-course of antagonism of NMDAR-mediated EPSCs by bath application of AP5 (20μM) measured with normal (grey) and MK801-containing (blue) pipettes. Note that NMDAR-mediated EPSCs are significantly reduced by the presence of MK801 in the patch pipette. All NMDARs were blocked with AP5 immediately prior to measuring AMPAR-mediated EPSCs shown in *Figure 3K* and *Figure 8L*.

ns p>.05; * p<.05; ** p<.01; ***p<.001 one-way ANOVA and Dunnett's multiple comparisons test and/or Student's t-test, two-tailed (*B-D*), and two-way repeated measures ANOVA (*G*).

Supplemental Figure 5

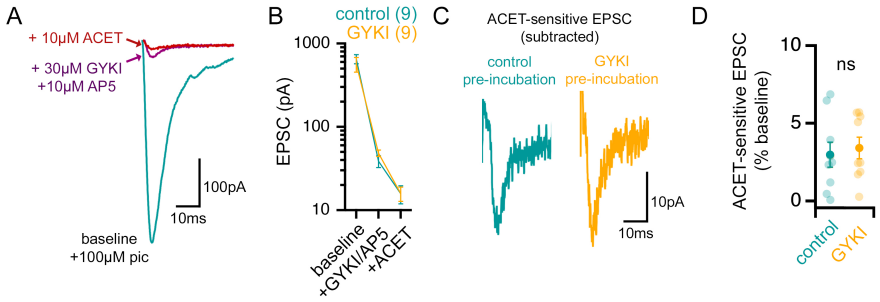

Supplemental Figure 5, related to Figure 3. ACET-sensitive currents do not substantially contribute to the measured EPSC

(**A**) Representative traces of EPSCs after bath application of GYKI (30μM) and AP5 (20μM) to block all AMPAR and NMDAR-mediated neurotransmission, and after ACET (10μM) to block KAR-mediated neurotransmission. (**B**) Mean ± SEM of EPSC amplitudes after acute application of GYKI and AP5 and ACET to the bath in slices that had been pre-incubated ± GYKI (5μM). (**C**) Representative traces of subtracted ACET-sensitive EPSCs. (**D**) The amplitude of ACET-sensitive EPSCs normalized to the amplitude of the baseline EPSC.

ns $p>.05$ Student's t-test, two-tailed. control n = 9 cells from 5 mice; GYKI n = 9 cells from 5 mice.

Supplemental Figure 6

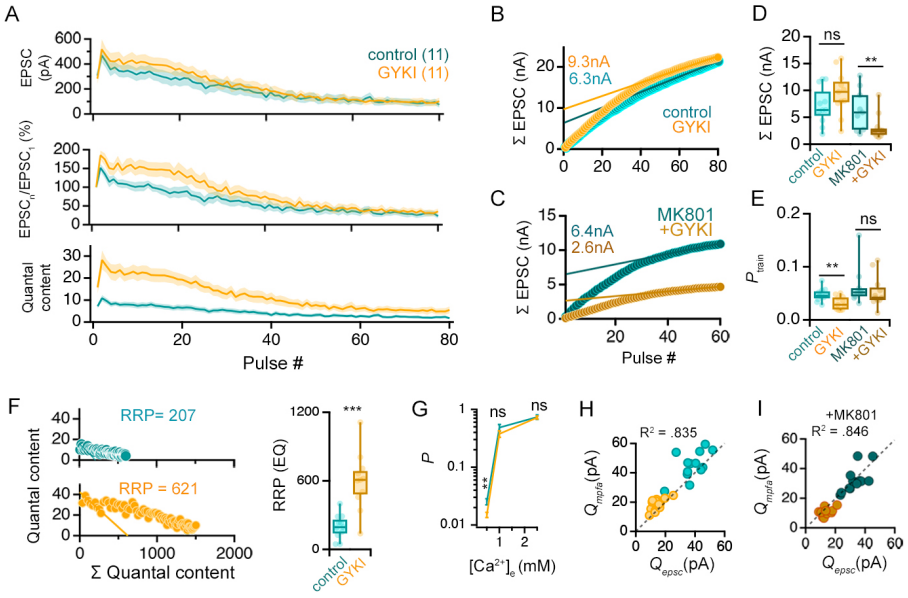

Supplemental Figure 6, related to Figure 5. Readily-releasable pool and release probability estimation using multiple probability fluctuation analysis

(**A)** At top, profiles of mean (± SEM) EPSC amplitudes, at middle, EPSC amplitudes normalized to the first EPSC in the train (% $EPSC_n/EPSC_1$), and at bottom, quantal contents (QC = $EPSC_n/Q_{mpfa}$) during 20Hz train stimulation. Experiments were performed in 2.5mM $[Ca^{2+}]_e$. (**B-C**) Estimations for RRP size based on cumulative EPSC amplitudes (∑EPSC) ± MK801 (10μM). (**D**) RRP size expressed as cumulative EPSCs. (**E**) Estimates of vesicle release probability from RRPs obtained by normalizing the quantal content of the first pulse in the train to the RRP estimate (P_{train}). (**F**) Estimation of RRP via the 'EQ' model (Elmqvist and Quastel, 1965), plotted as RRP size. Quantal content estimates were obtained by normalizing EPSCs and ∑EPSCs to Q_{epsc}s, derived by prior recordings in low $[Ca^{2+}]_e$. Pool size was estimated by extrapolating a linear fit of the rapid depression of EPSCs or QCs (the first 5-10 pulses immediately following short-term facilitation) to the X axis. (**G**) The binomial parameter, *P* obtained via multiple probability fluctuation analysis (MPFA) as shown in *Figure 5*. (**H-I**) MPFA-derived estimates of quantal amplitude (Q_{mpfa}) are linearly correlated with direct measurements of quantal amplitudes (Q_{espc}) under low (0.5mM) $[Ca^{2+}]_e$ conditions and in the presence of MK801 (10μM). R^2 values are the result of Pearson's correlation. Dashed lines indicate a slope of 1.

ns p>.05; ** p≤.01; ***p<.001 one-way ANOVA and Dunnett's multiple comparisons test (*D, G*), Kruskal-Wallis ANOVA and Mann-Whitney tests (*E*), or Student's t-test (*F*).

Supplemental Figure 7

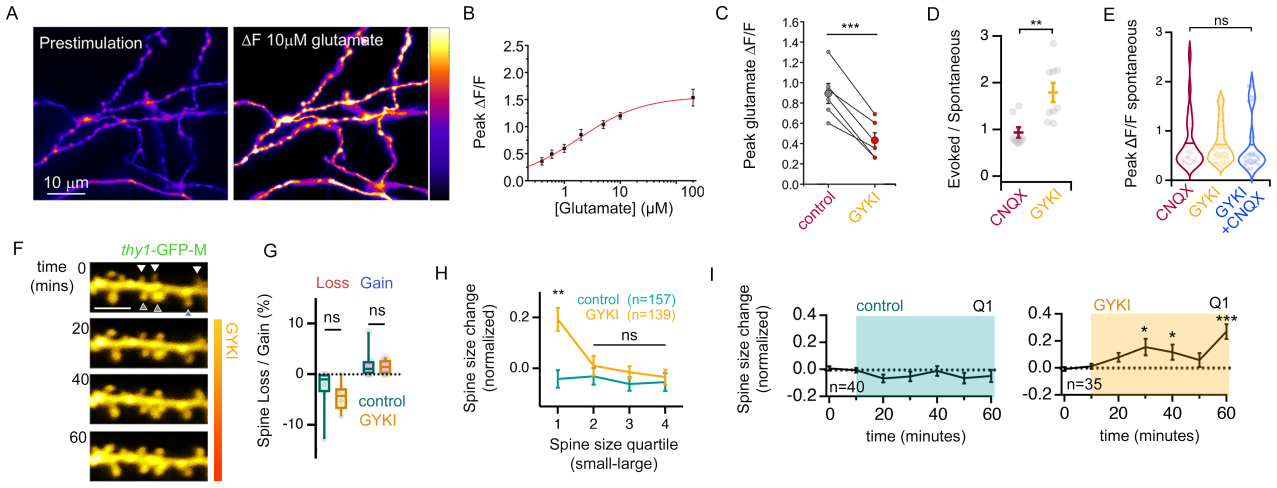

Supplemental Figure 7, related to Figure 6, 7. Characterization of iGluSnFR and dendritic spine analysis

(**A**) Pre- and post-stimulation images of a neuron expressing hsyn-iGluSnFR-A184S in response to a 10 μM glutamate puff. (**B**) Peak GluSnFR responses plotted against the concentration of glutamate delivered in the puff. Red line is a sigmoidal fit from a Hill function. (**C**) Peak glutamate response is decreased in GYKI-treated cells using the iGluSnFR-A184S reporter. This observation prompted us to perform the single bouton quantal analysis for this version of the optical glutamate reporter shown in *Figure 6C-F*. (**D**) Optical quantal contents (Evoked/Spontaneous) obtained from CNQX (10μM) or GYKI (5μM)-treated cultures. All boutons of a single cell were pooled together and averaged to generate a single data point (grey). Coloured markers show grand average ± SEM. CNQX n = 31 boutons from 8 cells; GYKI n = 25 boutons from 9 cells (see also *Figure 6F*). (**E**) Peak amplitude of spontaneously occurring GluSnFR3 signals in cultures treated with CNQX alone, GYKI alone, or CNQX+GYKI. CNQX n =27 boutons from 6 cells, GYKI n = 47 boutons from 8 cells, CNQX+GYKI n = 20 boutons from 6 cells. (**F**) Time-lapse imaging of spines along segments of secondary or tertiary dendrites in the *stratum oriens* during the application of GYKI (5μm). White arrows identify small spines that grow, black arrows identify mature spines that remain unchanged +GYKI. Scale bar = 2.5 μm. (**G**) Quantification of spine gain/loss as a fraction of the total baseline number of spines along a dendritic segment expressed as the total accrued over the 1 hour imaging session. To qualify as a loss, identified spines were lost for the entirety of the remaining imaging session. To qualify as a gain, spines appeared where none had existed before, and remained for the duration of the remaining imaging session. Control N = 6 dendritic segments (26.6 ± 1.4 μm; range 24-49 spines/segment); GYKI N = 6 dendritic segments (26.1 ± 2.4 μm; range 24-38 spines/segment) from 3 mice. (**H**) Normalized spine volume changes binned into baseline size quartiles. Spine size change is the % difference of the average of the last three images (t = 40, 50, 60 mins) as compared to its average baseline size (t = 0, 10 mins). The 1rst quartile encompasses the smallest 25% of spines for each condition, etc. Control, n = 157 spines from 8 dendritic segments (~20 measured spines/segment) from 3 mice; GYKI, n = 139 spines from 7 dendritic segments (~20 measured spines/segment) from 3 mice. Only one dendritic segment was imaged per slice. (**I**) The smallest quartile of spines at baseline (Q1) preferentially increase in size within 1 hours of GYKI wash-on.

ns p>.05; *p<.05, ** p<.01, ***p<.001 unpaired two-tailed t-tests (*C, D, I*), one-way Kruskal-Wallis ANOVA and Dunn's multiple comparisons test (*E, G*), one-way repeated measured ANOVA and Dunnett's multiple comparisons test (*K*), or Kolmogorov Smirnov test (*J*).

Supplemental Figure 8

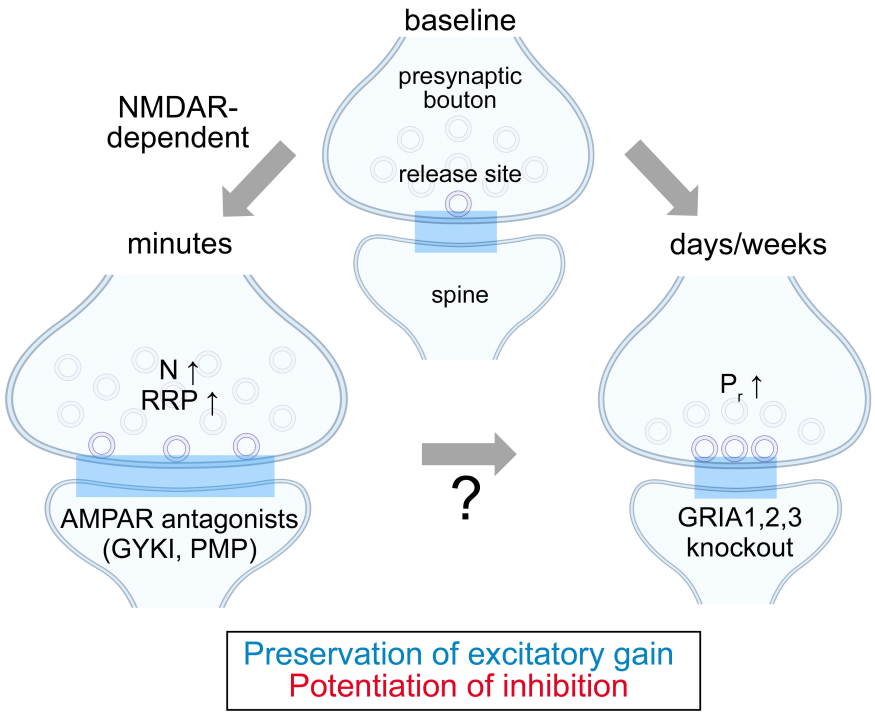

Supplemental Figure 8, related to Figures 1-8. Summary Model

AMPAR-specific antagonism (arrow to left lower synapse) results in a rapid (within minutes) NMDAR-dependent increase in the number of glutamate release sites, reflected ultrastructurally as an expansion of the active zone and an increase in the number of docked synaptic vesicles. The homeostatic potentiation of excitatory gain is paralleled by the potentiation of inhibitory synaptic transmission, ultimately favoring network inhibition. Postsynaptic genetic depletion of AMPARs *in vivo* (arrow to right lower synapse) results in a sustained (days to weeks) compensatory enhancement of synaptic release probability that offsets the reduction in postsynaptic strength. It remains unknown whether the two responses (rapid and sustained) are linked, or whether they represent separate phenomena.